Impact of injection rate on transient oil recovery under mixed-wet conditions: a microfluidic study

Magali Christensen, Xanat Zacarias-Hernandez, Yukie Tanino
School of Engineering, University of Aberdeen, UK

This paper was prepared for presentation at the International Symposium of the Society of Core Analysts held in Trondheim, Norway, 27-30 August 2018

ABSTRACT

Lab-on-a-chip methods were used to visualize the pore-scale distribution of oil within a mixed-wet, quasi-monolayer of marble grains packed in a microfluidic channel as the oil was displaced by water. Water injection rates corresponding to microscopic capillary numbers between Ca = 5 $\times 10^{-8}$ and 2 $\times 10^{-4}$ (Darcy velocities between 0.3 and 1100 ft/d) were considered. As expected, early-time water invasion transitions from stable displacement to capillary fingering with decreasing Ca, with capillary fingering observed at Ca $\leq 10^{-5}$. End-point oil saturation decreases with Ca over the entire range of Ca considered, consistent with the canonical capillary desaturation curve. In contrast, S_{or} derived from approximate numerical simulations using reasonable $P_c(S_w)$ do not display a strong dependence on Ca. These results suggest that the Ca dependence of end-point oil saturation is largely due to capillary end effects which, under conditions considered presently, affect the entire length of the packed bed.

INTRODUCTION

Invasion of a non-wetting phase into a porous medium saturated with a wetting phase has been studied extensively in numerical simulation (e.g., [1]) and experiments using idealized 2D or quasi-2D microfluidic devices [*e.g.*, 2, 3, 4, 5, 6]. Most of these studies have considered conditions characteristic of primary drainage that is, the invasion of the non-wetting phase occurs in a porous medium fully saturated with the wetting-phase, and pore-scale displacement mechanisms under these conditions have been stablished [1, 2, 7, 8]. In contrast, less attention has been given to secondary drainage relevant to oil recovery from oil-wet reservoirs and groundwater remediation, where the medium is partially saturated with the invading fluid.

In this paper we present laboratory observations of oil displacement from mixed-wet beds of crushed marble by water injection. We focus on injection velocities corresponding to microscopic capillary numbers between Ca = 5 $\times 10^{-8}$ and 2 $\times 10^{-4}$. Contrary to idealized geometrical micromodels, the packed beds used in this study preserve grain surface roughness, intra-grain mineral heterogeneity and a relatively large grain size distribution. Three invasion regimes are identified based on footprints observed at early-time and post-breakthrough displacements. Front propagation dynamics, "average" oil saturation, and their dependence on flow regime are discussed. The significance of capillary end effects are assessed by comparing observed end-point saturations to residual oil saturation estimated from numerical simulations.

MATERIALS

Microfluidic carbonate analogues

Displacement experiments were performed on quasi-monolayers of unconsolidated white marble grains (mean equivalent diameter of 53 ± 24 μm [11]) packed in a W = 1200 μm-wide, H = 55 μm-deep channel etched in soda lime (Dolomite Centre Ltd.). The porosity and permeability of the packed beds were ϕ = 0.27 [9] and k = 690 mD [10], respectively. The length of the packed beds ranged from L = 1540 to 2250 μm (Table 2). Fresh grains were used for each experiment to avoid any ambiguity in wettability. Details of the grain preparation and packing method are reported in Refs. [10, 11] and are thus omitted here.

Fluids

The brine was a solution of 5 wt.% NaCl and 1 wt.% KCl saturated with limestone, as used previously in Refs. [10, 12, 13, 14, 15, 16, 17]. The oil was a 6.6×10^{-2} M solution of cyclohexanepentanoic acid in *n*-decane dyed with Oil Red O (ORO) at a concentration of 9×10^{-4} M [10]. The corresponding interfacial tension and static contact angle on a polished marble substrate are σ = 19.3 ± 0.1 mN/m and θ_s = 138 ± 3°, respectively [16]. The density, ρ, and viscosity, μ, of the test fluids are summarized in Table 1.

Table 1. Basic properties of the brine and test oil at T = 21°C.

test fluid	ρ [kg/m^3]	μ [mPa s]
brine [17]	1040.2	1.109
6.6×10^{-2} M cyclohexanepentanoic acid + ORO [16]	732.9	0.899

METHODS

Displacement experiments

The procedure combines the coreflood protocol developed by Tanino & Blunt [12, 13], lab-on-a-chip methods developed by Bowden *et al.* [11, 18], and the visualization method developed by Tanino *et al*. 2018 [10]. The experimental setup is the same as that in Tanino *et al*. [10] (Fig. 1).

The displacement sequence consisted of two steps. First, oil was injected into a brine-saturated packed bed to establish initial oil saturation S_{oi} = 0.97 ± 0.03 [10], and left to age between t_a = 50 to 81 h. Second, brine was injected using a high-precision microfluidic syringe (pump 11 elite nanomite, Harvard Apparatus) at a constant volumetric flow rate Q_w. The combination of the high S_{oi} and large contact angle resulted in a predominantly oil-wet packed bed where waterflood was a secondary drainage process rather than imbibition.[1]

In the present paper, we consider injection rates between $Q_w = 3.7 \times 10^{-3}$ and 15 μL/min, which correspond to Darcy velocities of $U_w = Q_w/A$ = 0.95 to 3900 μm/s (Table 2). The corresponding capillary numbers fall between $Ca = 5.5 \times 10^{-8}$ and 2.2×10^{-4}. With a viscosity ratio of μ_w/μ_o = 1.2, these values of Ca extend from the capillary fingering-dominated regime to the transitional regime between stable displacement and capillary fingering as determined for primary drainage in the network of capillaries considered by Lenormand *et al*. [1] and microfluidic cylinder arrays

[1] Whether the organic acid alters the interfacial tension only or whether it also alters the surface of the grains – and if so, whether this reaction is permanent or reversible – remains an open question.

by Zhang *et al*. [2] (Fig. 2).

Table 2. Summary of the displacement experiments. $\langle S_{ob} \rangle$ and $\langle S_{oe} \rangle$ were previously reported in Ref. [16].

run	**Δt** [ms]	**L** [μm]	**U_w** [μm/s]	**Ca**	**$\langle S_{ob} \rangle$** [16]	**$\langle S_{oe} \rangle$** [16]
M14	30	1910	3860	2.2×10^{-4}	0.60 ± 0.008	0.48 ± 0.01
M21	100	1880	1550	8.9×10^{-5}	0.57 ± 0.03	0.45 ± 0.02
M11	30	1870	1550	9.1×10^{-5}	0.67 ± 0.02	0.50 ± 0.02
M17	50	1680	773	4.6×10^{-5}	0.73 ± 0.06	0.55 ± 0.03
M5	100	1870	260	1.5×10^{-5}	0.62 ± 0.04	0.62 ± 0.04
M7[a]	100	2440	26	1.5×10^{-6}	0.61 ± 0.02	0.62 ± 0.02
M8	100	2250	26	1.5×10^{-6}	0.60 ± 0.02	0.66 ± 0.03
M6	100	1540	0.95	5.5×10^{-8}	0.68 ± 0.01	0.72 ± 0.04

[a] This experiment was first analyzed in Ref. [9] using a more basic post-processing algorithm.

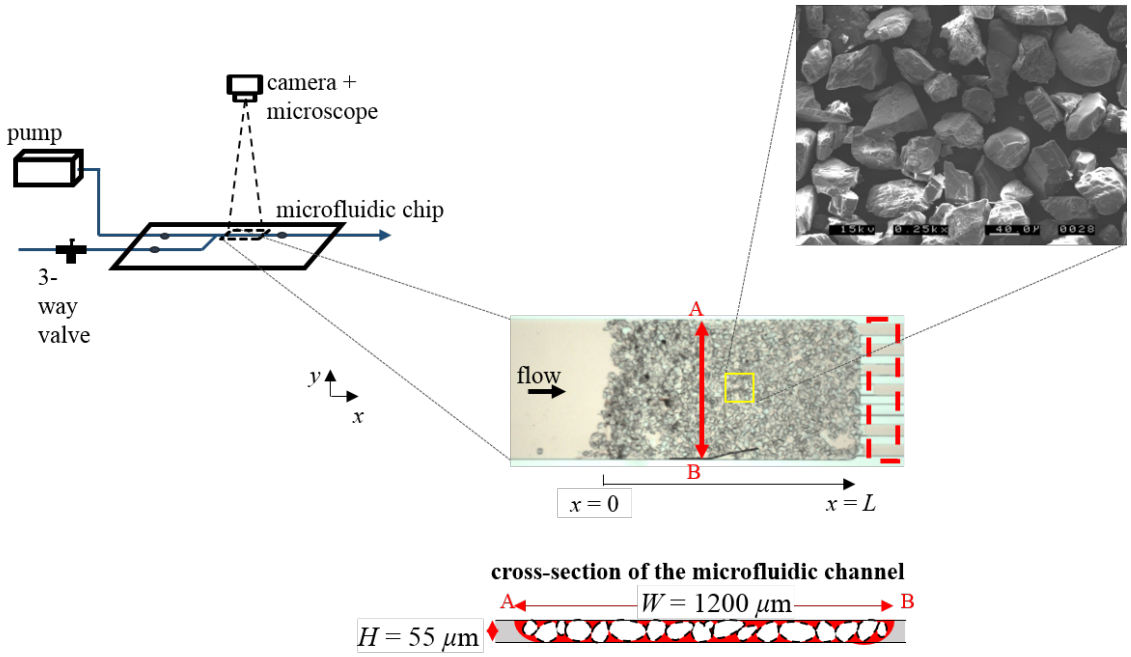

Figure 1. The microfluidic setup (left) and scanning electron microscope (SEM) image of the grains (right). The dashed red rectangle demarcates the region downstream of the packed bed used to identify water breakthrough.

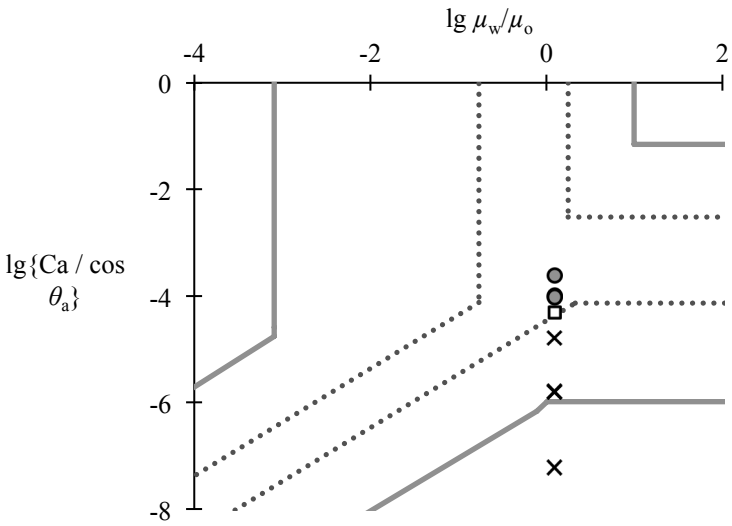

Figure 2. Mobility ratio-Ca regime map. Marker shapes depict flow patterns observed in the displacement experiments: capillary fingering (cross), stable displacement (solid circle), and post-breakthrough sweep (squares), Superposed are regime boundaries for primary drainage proposed in the literature for uniformly wetting micromodels: a network of capillaries ([1], grey solid line) and a uniform cylinder array ([2], grey dotted). Adapted from [16].

Depth-averaged oil saturation and front progression

The packed bed was back-lit using a variable wavelength light source (Lumen 1600-LED, Prior Scientific), and the depth-integrated fluid distribution was imaged using a high-speed 24-bit colour camera (Pixelink PL-B742F) coupled to an optical microscope (Nikon SMZ745T) in a sequence of RGB images. The exposure time ranged from Δt = 30 to 100 ms depending on the injection rate (Table 2); the image resolution was 3.0 μm/pix.

Depth-averaged saturation was extracted from the ratio of the blue channel intensity to the red channel intensity, $i_B(x,y,t)/i_R(x,y,t)$, in each pixel following the protocol proposed by Christensen *et al*. [16]. In brief:

1. The ratio i_B/i_R was extracted from each image.
2. A spatial 3 × 3 median filter was applied.
3. i_B/i_R was further normalized by i_B/i_R on either side of the microfluidic channel to correct for instantaneous fluctuations in incident light.

The mean oil saturation is then given by

$$\langle S_o \rangle(t) = \frac{1-\langle i_B/i_R \rangle}{1-\langle i_B/i_R \rangle_{min}} , \quad (1)$$

where angular brackets denote a spatial average over $x \pm H$ and L (Fig. 1). All post-processing was performed in MATLAB (Mathworks, Ltd.).

Numerical simulation

Approximate numerical simulations of the experiments were performed using core analysis software CYDAR^{TM} (CYDAREX). Imbibition capillary pressure, $P_c^C(S_w^*)$, measured on the same rock (Indiana limestone) by centrifuge [20], was used in the simulations after rescaling according to the Leverett-J function to account for differences in ϕ and k:

$$P_c(S_w^*) = P_c^C(S_w^*)\sqrt{\frac{k^C/\phi^C}{k/\phi}}\,, \tag{2}$$

where superscript C denotes properties of the core used in the centrifuge experiment and

$$S_w^* = \frac{S_w - (1 - S_{oi})}{(1 - S_{or}) - (1 - S_{oi})} \tag{3}$$

is water saturation normalized to account for differences in S_{oi}. Irreducible water saturation was taken to be $S_{wi} = 0$ in all simulations to reduce the number of fitting parameters. S_{or} and relative permeabilities, modelled using Brooks-Corey correlations [21]:

$$k_{rw} = k_{rw}(S_{or})\, S_w^{*\alpha_w}\,, \quad k_{ro} = k_{ro}(S_{wi})\,(1\text{-}S_w^*)^{\alpha_o}, \tag{4}$$

where S_{or}, α_w ($\geq$1), α_o ($\geq$1), $k_{rw}(S_{or})$, and $k_{ro}(S_{oi})$ were fitting parameters, were extracted by iterative history matching of simulated packed bed-averaged oil saturation, $\langle S_o \rangle(t)$, to measured values.[2]

RESULTS

Water invasion dynamics

Figure 3 presents snapshots of the packed bed at three instances during five waterfloods: $\tilde{t} = \frac{3}{4}\tilde{t}_b$, $\tilde{t}_b$, and $\tilde{t}_b + 100$, where $\tilde{t}_b$ denotes water breakthrough time and the tilde denotes time normalized by the cumulative volume of water injected, $\tilde{t} = t\ U_w / (L\ \phi)$.

At the largest Ca (= 2.2×10^{-4}), the invading water front is compact and relatively flat across the entire width of the channel, characteristic of stable displacement as identified by Lenormand *et al*. [1]. At water breakthrough, the largest pockets of oil only span ~$3d_p$. After breakthrough, water saturation increases along the entire length of the packed bed, but oil-occupied pores remain largely so. This suggests that additional oil was displaced from already swept pores, at length scales below or comparable to the image resolution.

At low Ca $\leq 2 \times 10^{-5}$, fingers form at the onset of water invasion (bottom two rows). As is typical of drainage, water first bursts through the centre of larger pores, then expands outwards towards corners and into adjacent, smaller pores. Fingers propagate laterally as well as backwards, characteristic of capillary fingering (arrows). After breakthrough, clusters that remain bypassed generally remain so (yellow polygons); presumably the applied (macroscopic) pressure gradient is insufficient to exceed the capillary entry pressures of oil-occupied pores, and water simply flows through the network of water-invaded pores without displacing additional oil.

In between ($4.6 \times 10^{-5} \leq$ Ca $\leq 9.1 \times 10^{-5}$), the invasion behaviour transitions between the two regimes (second and third rows). At early times, the invading water front is less flat, and fingering is observed at the lower limit (arrows, Ca = 4.6×10^{-5}). Bypassed oil clusters vary in size from the order a pore diameter to almost half the channel width. Furthermore, this Ca

[2] Pressure measurements are not available for these experiments. Because only production volumes were used in the history matching, the extracted best-fit relative permeability curves may not necessarily be a unique solution.

regime is characterized by water invasion into initially bypassed, large clusters after breakthrough (dotted white polygons).

In the present experiments, capillary fingering emerges at a critical Ca of $Ca_c = O(10^{-5})$, which is about an order of magnitude larger than that observed for a Berea sandstone [22]. However, Ca_c is expected to be a function of the porous medium as well as wettability [23].

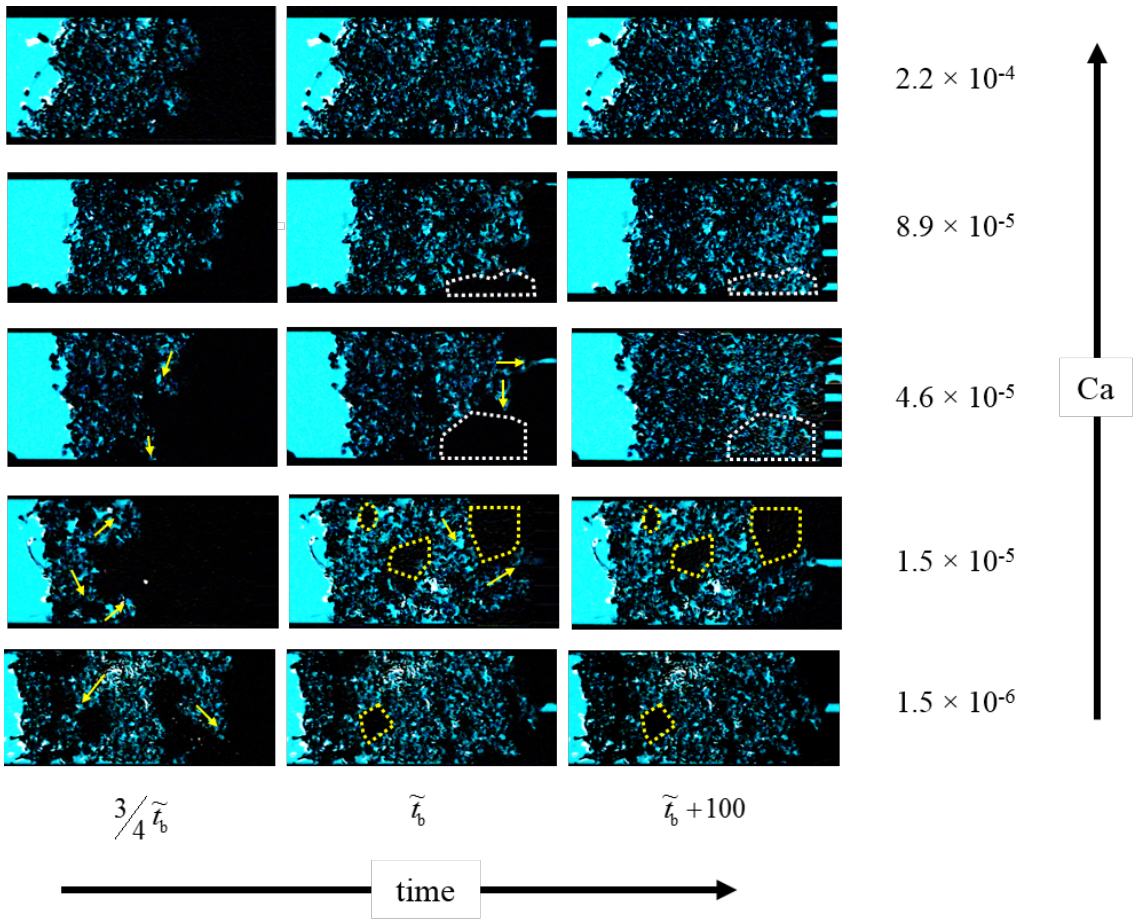

Figure 3. Snapshots of the packed bed at $\tilde{t} = 3\tilde{t}_b/4$, $\tilde{t}_b$, and $\tilde{t}_b + 100$. An image at the onset of waterflood has been subtracted from each image and a 2 × 2 median filter applied; bright pixels represent invading water. Imposed flow is from left to right. White dotted polygons demarcate regions invaded by water only after breakthrough. Yellow dotted polygons demarcate regions that remain unswept throughout the duration of the waterflood. Yellow arrows depict the direction of finger propagation as determined by visual inspection. From top to bottom: experiment M14, M21, M17, M5, and M7 (Table 2). Adapted from Ref. [16].

The packed bed-averaged water saturation, $\langle S_w \rangle$, is presented as a function of time in Fig. 4 for selected waterfloods. It is readily apparent that as Ca increases (left to right), end-point $\langle S_w \rangle$ increases, i.e., remaining oil saturation decreases, consistent with the classic capillary desaturation curve (e.g., Fig. 5).

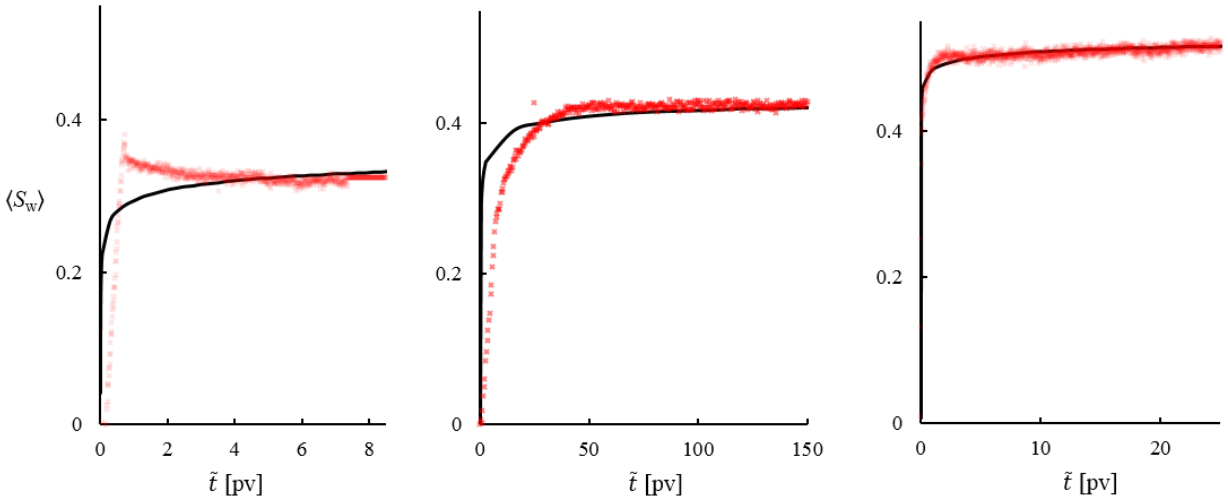

Figure 4. Evolution of the remaining oil saturation as measured in the packed bed (red ×) and simulated by history matching (solid line) for Ca = 1.5×10^{-6} (left, M8), 4.6×10^{-5} (middle), and 2.2×10^{-4} (right). Where the solid line is not visible, it overlaps with the markers.

Note that at Ca = 1.5×10^{-6}, $\langle S_w \rangle$ decreases after breakthrough. This is a salient feature of the lowest Ca waterfloods; visual inspection of the images indicates that this is due to the counter-current imbibition of produced oil from the downstream end of the packed bed.

Capillary desaturation

Figure 5 presents the classic capillary desaturation curve: packed bed (or core)-averaged end-point saturation, normalized by its value at the lowest Ca, as a function of Ca. Superposed are coreflood data from the literature previously compiled by Tanino *et al*. [24]. It is readily apparent that the end-point packed bed-averaged oil saturation, $\langle S_{oe} \rangle$, decays with increasing Ca throughout the range of values considered (red triangles). Interestingly, there is no evidence of a Ca-independent regime at low Ca documented for (uniformly) water-wet conditions. The absence of a Ca-independent regime is, however, consistent with coreflood measurements on Whitestone and Edwards limestone by Tie & Morrow [25] under mixed-wet conditions (open red markers, Fig. 4).

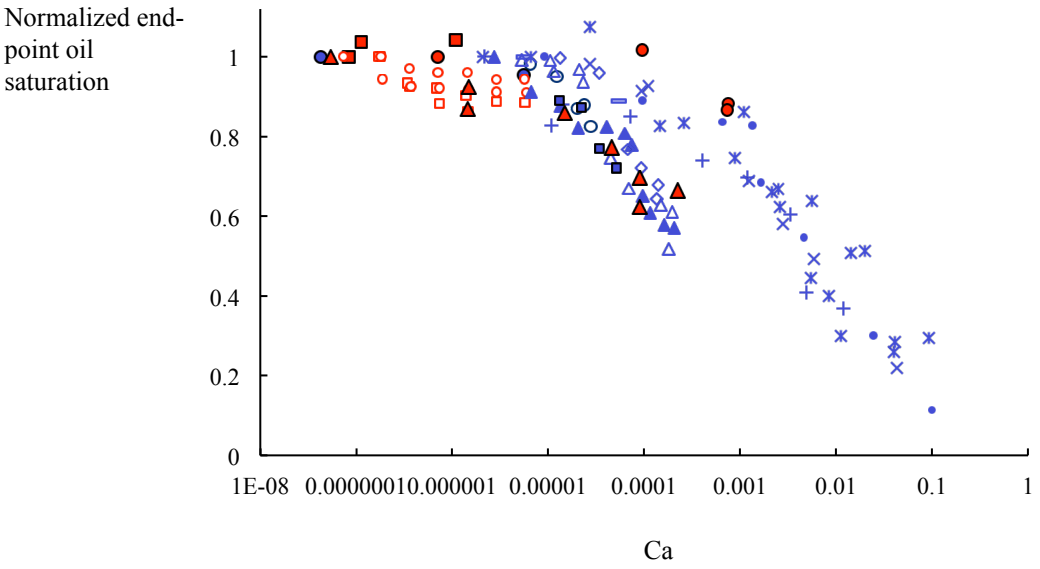

Figure 5. End-point oil saturation normalized by its maximum value as a function of Ca under mixed-wet conditions (red) and uniformly water-wet conditions (blue) measured in Ketton (solid circle) and Indiana (solid square) limestones [24], in Whitestone and Edwards limestones by Tie & Morrow [25], in Berea sandstone by Chatzis & Morrow [23], and in five sandstones by Abrams [26] and $\langle S_{oe} \rangle$ from the present study (red triangles). Expanded from Tanino *et al.* [24].

Impact of capillary end effects

Finally, we use the numerical simulations to evaluate the significance of capillary end effects. A satisfactory match between simulated and measured saturation is achieved for most experiments, even though early time behaviour in not well captured at low Ca (e.g., Fig. 4).

The best-fit coefficients for the Brooks-Corey correlations derived from history matching are summarized in Table 3. Counter-intuitively, $k_{rw}(S_{or})$, $k_{ro}(0)$, α_w, and α_o do not display a strong dependence on Ca. However, without pressure drop and five fitting parameters, the best-fit $k_r(S_w)$ curves may be one of the many that can match the production data. A more robust interpretation requires measurement of both pressure and oil saturation, which is an ongoing effort.

Table 3. Summary of history matching of selected microfluidic waterfloods. We were unable to achieve satisfactory agreement between simulation and measured data for M7 and M6.

run	Ca	S_{or}	$k_{rw}(S_{or})$	α_w	$k_{ro}(0)$	α_o
M14	2.2×10^{-4}	0.57	0.11	6.8	0.98	6.7
M11	9.1×10^{-5}	0.58	0.10	10	0.12	4.5
M21	8.9×10^{-5}	0.57	0.27	6.7	0.27	1.8
M17	4.6×10^{-5}	0.57	0.41	0.1	0.10	3.3
M5	1.5×10^{-5}	0.56	0.10	8.7	0.05	2.2
M8	1.5×10^{-6}	0.46	0.24	7.8	0.05	7.8

Figure 6 presents the simulated equilibrium (end-point) saturation profiles for selected waterfloods. At the downstream end of the packed bed, oil, which is the wetting phase for most

of the grain surfaces, is retained by capillary forces giving rise to the sharp drop in S_w near $x = L$. The extent of this region of rapidly changing S_w broadly increases with decreasing U_w. Nevertheless, under the conditions considered presently, capillary end effects span the entire length of the packed bed.

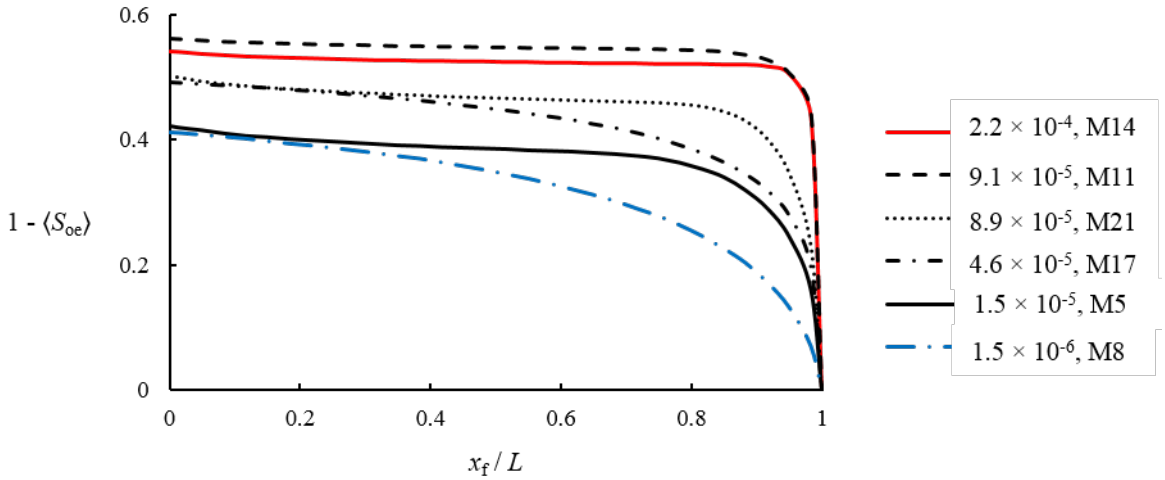

Figure 6. End-point water saturation along the length of the packed bed at selected Ca: Ca = 1.5×10^{-6} (blue dash-dotted), 1.5×10^{-5} (black solid), 4.6×10^{-5} (black dotted-dashed), 8.9×10^{-5} (black dotted), 9.1×10^{-5} (black dashed), 2.2×10^{-4} (red solid).

Contrary to $\langle S_{oe} \rangle$ measured in the present experiments and in an array of cylinders by Zhang *et al.* [2], S_{or} estimated from history matching only displays a weak dependence on Ca, with S_{or} becoming Ca independent at Ca ~ 10^{-5} (Fig. 7). The difference between $\langle S_{oe} \rangle$ and S_{or} increases with decreasing Ca, which is attributed to two factors. First, physical reasoning suggests that capillary end effects become less significant as Ca increases. Second, premature termination of the waterflood may affect lower Ca.

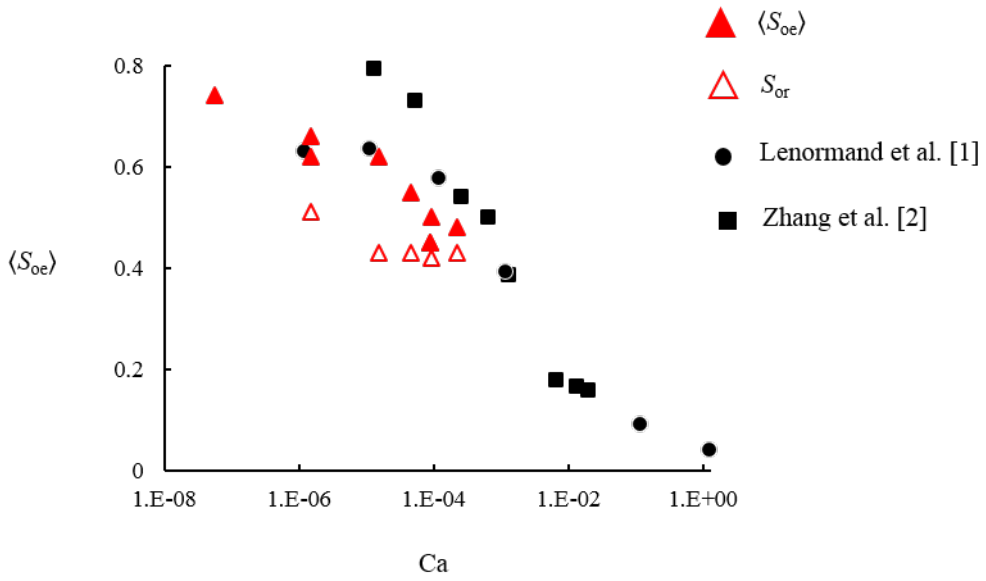

Figure 7. ⟨S_{oe}⟩ (solid triangles) and S_{or} estimated from history matching (open) as a function of Ca, plotted along measurements by Lenormand *et al*. [1] and Zhang *et al.* [2].

CONCLUSIONS

We presented depth-averaged distributions of oil in a quasi-monolayer of marble grains packed in a microfluidic channel as it was displaced by brine from maximum initial oil saturation. S_{or} was extracted by matching simulation to measured oil production by adjusting $k_{rw}(S_w)$, $k_{ro}(S_w)$, and $P_c(S_w)$. The main findings are:

- Under conditions considered presently, capillary fingering occurs at Ca $\leq 10^{-5}$.
- Simulations suggest that capillary end effects span the entire length of the packed bed [O(1.5 to 3) mm] at all capillary numbers considered (Ca $\leq 2 \times 10^{-4}$).
- As expected, the difference between bed-averaged end-point oil saturation established by waterflood and best-fit S_{or} estimated from history matching increases with decreasing Ca.
- Bed-averaged end-point saturation decreases with Ca over the entire range of Ca considered. In particular, a Ca-independent regime is not observed at low Ca.
- S_{or} does not display a strong dependence on Ca.

The above results highlight the importance of using simulation to interpret micromodel experiments after water breakthrough. We are not aware of any micromodel study of two-phase flow in the literature that do so.

ACKNOWLEDGEMENTS

This paper contains work supported by the Royal Society Research Grant RG140009. MC was supported by a University of Aberdeen College of Physical Sciences scholarship. XZH is supported by the Mexican National Council for Science and Technology (CONACyT). The authors thank Olalekan Ajayi for unpublished SEM images, Guillaume Lenormand at CYDAREX for helpful suggestions on their software CYDAR™, COREX (UK) Ltd. for allowing MC access to their viscometer, and Paul Hallet for allowing MC access to their tensiometer.

REFERENCES

1. Lenormand, R., E. Touboul & C. Zarcone (1988) Numerical models and experiments on immiscible displacements in porous media. *J. Fluid Mech.*, *189*, 165-187.
2. Zhang, C., M. Oostrom, T. W. Wietsma, J. W. Grate & M. G. Warner (2011) Influence of viscous and capillary forces on immiscible fluid displacement: Pore-scale experimental study in a water-wet micromodel demonstrating viscous and capillary fingering. *Energy Fuel*, *25*(8), 3493-3505.
3. Zhao, B., C. W. MacMinn & R. Juanes (2016) Wettability control on multiphase flow in patterned microfluidics. *Proc. Nat. Acad. Sci*, *113*(37), 10251-10256.
4. Xu, W., J. T. Ok, F. Xiao, K. B. Neeves & X. Yin (2014) Effect of pore geometry and interfacial tension on water-oil displacement efficiency in oil-wet microfluidic porous media analogs. *Phys. Fluids*, *26*(9), 093102.
5. Cottin, C., H. Bodiguel & A. Colin (2010) Drainage in two-dimensional porous media: From capillary fingering to viscous flow. *Phys. Rev. E*, *82*(4), 046315.
6. Zheng, X., N. Mahabadi, T. S. Yun & J. Jang (2017) Effect of capillary and viscous forces on CO_2 saturation and invasion pattern in microfluidic chip. *J. Geophys. Res. Solid Earth*, *122*, 1634-1647.
7. Wilkinson, D. & J. F. Willemsen (1983) Invasion percolation: a new form of percolation theory. *J. Phys. A: Math. Gen.*, *16*(14), 3365.
8. Homsy, G. M. (1987). Viscous fingering in porous media. *Annu. Rev. Fluid. Mech.*, *19*(1), 271-311.
9. Tanino, Y., M. Christensen & X. Zacarias Hernandez (2017) Residual oil saturation under mixed-wet conditions: a direct comparison between Indiana limestone and its microfluidic analogue. *Proc.* International Symposium of the Society of Core Analysts, 27 Aug. -1 Sept., SCA2017-009, Vienna, Austria.
10. Tanino, Y., X. Zacarias-Hernandez & M. Christensen (2018) Oil/water displacement in microfluidic packed beds under weakly water-wetting conditions: competition between precursor film flow and piston-like displacement. *Exp. Fluids*, 59(2).
11. Bowden, S. A., Y. Tanino, B. Akamairo & M. Christensen (2016) Recreating mineralogical petrographic heterogeneity within microfluidic chips: assembly, examples, and applications. *Lab Chip*, *16*(24), 4677-4681.
12. Tanino, Y. & M. J. Blunt (2012) Capillary trapping in sandstones and carbonates: Dependence on pore structure, *Water Resour. Res.*, *48*(8).
13. Tanino, Y. & M. J. Blunt (2013) Laboratory investigation of capillary trapping under mixed-wet conditions, *Water Resour. Res.*, *49*(7), 4311–4319.
14. Christensen, M. & Y. Tanino (2017) Enhanced permeability due to apparent oil/brine slippage in limestone and its dependence on wettability, *Geophys. Res. Lett.*, *44*(12).
15. Christensen, M. & Y. Tanino (2017) Waterflood oil recovery from mixed-wet limestone: dependence on contact angle, *Energy Fuel*, *31*(2), 1529–1535.
16. Christensen, M., X. Zacarias-Hernandez & Y. Tanino (2018) Secondary drainage under mixed-wet conditions: crossover from stable displacement to capillary fingering in a microfluidic packed bed. *Adv. Water Res*, under review.
17. Romanello, L. (2015) Impact of wettability on relative permeability, MSc thesis, University of Aberdeen.

18. Bowden, S. A., J. M. Cooper, F. Greub, D. Tambo & A. Hurst (2010). Benchmarking methods of enhanced heavy oil recovery using a microscaled bead-pack. *Lab Chip*, *10*(7), 819-823.
19. Frette, O. I., K. J. Måløy, J. Schmittbuhl & A. Hansen (1997) Immiscible displacement of viscosity-matched fluids in two-dimensional porous media. *Phys. Rev. E*, *55*(3), 2969.
20. Christensen, M & Y. Tanino (2018) Residual oil saturation under mixed-wet conditions: optimal wettability revisited. *Proc.* International Symposium of the Society of Core Analysts, SCA2018-011, *under review*, Trondheim, Norway.
21. Brooks, R. & T. Corey (1964) Hydraulic properties of porous media. *Colorado State University Hydrology Papers*, 3.
22. Singh, M. & K. K. Mohanty (2003) Dynamic modeling of drainage through three-dimensional porous materials. *Chem. Eng. Sci.*, *58*(1), 1-18.
23. Chatzis, I. & N. R. Morrow (1984) Correlation of capillary number relationships for sandstone. *Soc. Petrol. Eng. J.*, *24*(05), 555-562.
24. Tanino, Y., B. Akamairo, M. Christensen & S. A. Bowden (2015) Impact of displacement rate on waterflood oil recovery under mixed-wet conditions. *Proc.,* International Symposium of the Society of Core Analysts. St. John's Newfoundland and Labrador, Canada, 16-21 Aug.
25. Tie, H. & N. R. Morrow (2005) Low-flood-rate residual saturations in carbonate rocks. *Proc*., International Petroleum Technology Conference, 21-23 Nov., Doha, Qatar.
26. Abrams, A. (1975) The influence of fluid viscosity, interfacial tension, and flow velocity on residual oil saturation left by waterflood. *Soc. Petrol. Eng. J.*, *15*(5), 437-447.